Title

Investigation of the interaction of a laser pulse with a preformed Gaussian Sn plume for an extreme ultraviolet lithography source

Permalink

https://escholarship.org/uc/item/65t9h4zw

Journal

Journal of Applied Physics, 101(2)

ISSN

0021-8979

Authors

Tao, Y
Tillack, M S
Harilal, S S
et al.

Publication Date

2007

Peer reviewed

Investigation of the interaction of a laser pulse with a preformed Gaussian Sn plume for an extreme ultraviolet lithography source

Y. Tao,[a] M. S. Tillack, S. S. Harilal, K. L. Sequoia, and F. Najmabadi

Department of Mechanical and Aerospace Engineering, University of California, San Diego,
9500 Gilman Drive, La Jolla, California 92093-0438 and the Center for Energy Research,
University of California, San Diego, 9500 Gilman Drive, La Jolla, California 92093-0438

The interaction of a laser pulse with a Sn preplasma formed by a low energy prepulse was investigated for an extreme ultraviolet (EUV) lithography light source. A much lower ion kinetic energy and nearly the same conversion efficiency from laser to in-band (2% bandwidth) 13.5 nm EUV light were simultaneously observed as compared with those from the direct interaction with a solid surface. The reason comes from the interaction of the laser pulse with a smooth preplume induced by the prepulse. The density profile of the preplume was measured with time-resolved shadowgraphy and could be fitted with a Gaussian function. The energy of the ions located at the flux peak E_p scales with the length of the preplume l_s as $E_p \propto 1/l_s$. Laser absorption in the low-density preplume and ion acceleration during plasma expansion are discussed. This result provides a general way to control particle energy from a laser plasma interaction. © *2007 American Institute of Physics*. [DOI: 10.1063/1.2426883]

I. INTRODUCTION

Extreme ultraviolet (EUV) lithography is one of the most promising next generation lithography tools succeeding the 193 nm optical lithography (using ArF laser) used in the semiconductor industry to produce electronic nodes with a critical size of 32 nm or less.[1] However, EUV lithography is facing several challenges for its application in high volume manufacture (HVM). One of those is to develop a powerful, clean, and long lifetime EUV light source. At present, most of the efforts focus on 13.5 nm EUV light with a bandwidth of 2% (in band) due to the availability of multilayer mirrors used in EUV lithography systems. Hot plasma, heated by an electric discharge or a high power laser, can efficiently emit 13.5 nm EUV light. Compared with discharge-produced plasma, laser-produced plasma has the advantages of high efficiency, cleanliness, and large collection angle. A laser-produced Sn plasma with a temperature around 30 eV provides the highest in-band conversion efficiency (CE) from laser to 13.5 nm EUV light due to its emission peak located at 13.5 nm.[2] However, debris becomes a critical issue for the use of Sn in a practical EUV lithography source for HVM. Fast particles with a kinetic energy of several keV have been observed from Sn plasmas. The fast particles could result in the permanent damage to the collector optics used in an extreme ultraviolet layer (EUVL) system. It has been shown that reduction of ion energy helps reduce the sputtering rate of the optics and to extend their lifetime.[3]

Ion acceleration in plasma has been described in terms of collisionless expansion into vacuum.[4] The initial conditions, such as ion density profile, play a key role in the plasma expansion. Theoretical efforts[5,6] have shown that electron cooling and wave breaking in the expansion of plasma with an initially smooth ion density profile may result

in slower ions as compared with a plasma with an initial infinitely sharp boundary. A prepulse is a convenient way to modify the initial density profile. The influence of a prepulse on ion acceleration in a high field has been investigated by theoretical and experimental efforts to increase ion energy and to improve beam quality. It has been shown that both the maximum energy and angular distribution depend on the level of the prepulse.[7,8] Ion acceleration is more efficient with a short initial scale length. A comparison between cases with and without a prepulse shows a variation in ion energies of a factor of 2–4.[7] Numerical simulations also suggested approximately two times reduction in velocity when a smooth initial ion density profile is considered.[5]

Recently we demonstrated a much larger reduction factor of 30 in ion energy from a laser-produced Sn plasma by introducing a low energy prepulse.[9] However, the mechanism dominating the phenomena was not clear until now. Further understanding of the effect of initial density profile on ion acceleration is not only necessary for the development of an EUV lithography source but also for other applications of laser plasma, such as laser ion acceleration, laser fusion, soft and hard x-ray sources, and pulsed laser deposition (PLD).

In this report, we present investigations to clarify the interaction of a laser pulse with a preformed Sn plasma, which are relevant to the properties of ions and in-band 13.5 nm EUV light emission. Even though most of our experiments have been carried out at the optimum conditions for a 13.5 nm EUV light source, these investigations are also helpful to understand the issues related to the general case of laser plasma interactions. This paper is organized as follows: Sec. II introduces the experimental arrangement for the measurements of ion spectrum, in-band CE, soft x-ray spectrum, and temporally resolved shadowgraphy and interferometry.
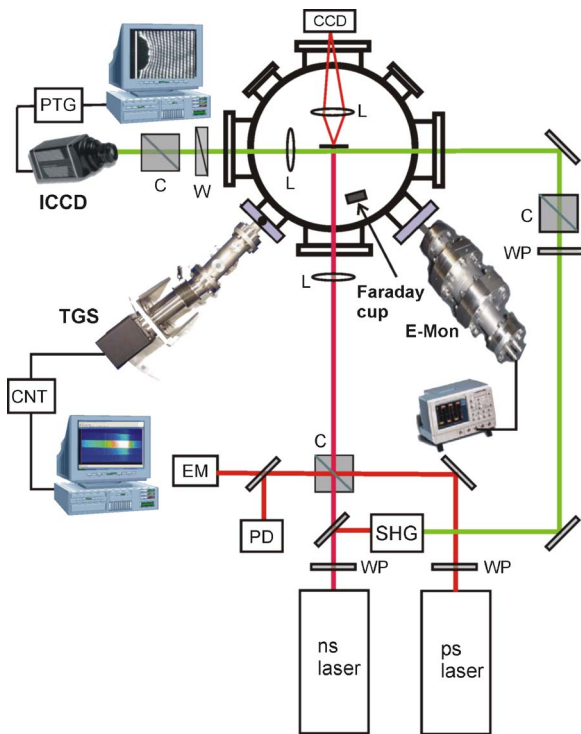
---

a)Electronic mail: yetao@ucsd.edu

FIG. 1. (Color online) Schematic of the experimental arrangement; WP-wave plate, C-cube polarizer, L-lens, SHG-second harmonic generator, W-Wollaston prism, PTG-pulse time generator, CNT-controller, EM-energy monitor, PD-photodiode, and TGS-transmission grating spectrometer.

Experimental results are shown in Sec. III, and laser absorption and plasma expansion are discussed in Sec. IV.

II. EXPERIMENTAL ARRANGEMENTS

A schematic of the experimental arrangement is illustrated in Fig. 1. Two lasers are employed in our experiments. One is a picosecond Nd: yttrium aluminum garnet (YAG) laser (EKSPLA SL335), which consists of one stimulated Brillouin scattering (SBS) oscillator and two stages of amplifiers. The Picosecond laser can produce a 1.064 μm laser pulse with pulse durations from 130 to 600 ps and pulse energy up to 500 mJ. The other is a 7 ns Nd:YAG laser (Continuum Surelite), which produces a 1.064 μm laser pulse with a maximum pulse energy of 650 mJ at 10 Hz. The picosecond laser is used as a prepulse. The nanosecond laser is used to generate the EUV plasma to match the optimized conditions for efficient generation of 13.5 nm EUV light,[10] called as the pumping pulse hereafter. The two lasers are synchronized with a pulse delay generator (Stanford DG535) with a jitter less than 0.5 ns. The two laser beams are combined into a collinear optical path by a cube polarizer. Energies of the two laser beams are independently adjusted by using two $\lambda/2$ wave plates placed in front of the cube polarizer. They are focused by a same lens with a focal length of 300 mm onto the surface of the target at normal incidence. The target is placed inside a vacuum chamber with a pressure below 10^{-6} Torr to avoid absorption of the EUV light induced by the remaining air. The size and the overlap of the two focal spots were measured by an optical image relay method. The focal spot sizes [full width at half maximum
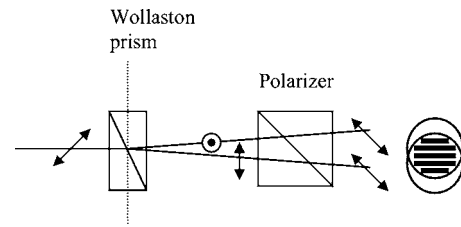
(FWHM)] of the pre- and pumping pulses are 300 and 100 μm, respectively. A bulk Sn slab is used as the target. The target is moved to maintain a new surface for each shot.

The plasma density profile is measured using a Nomarski interferometer. A small part split from the pumping pulse is converted into 0.532 μm light by a second harmonic generator (SHG) (type II KDP crystal) and used as a probe beam. A $\lambda/2$ wave plate and a cube polarizer are used to adjust the polarization and energy of the probe beam. The probe beam passes through the plasma parallel to the target surface and is relayed to an imager by a $F/15$ lens. The Nomarski interferometer is inserted in front of the imager. An optical schematic of the interferometer is illustrated in Fig. 2, consisting of a Wollaston prism with a split angle of 10 mrad and a cube polarizer. The polarization of the probe beam is rotated 45° with respect to the horizontal direction. The Wollaston prism splits the probe beam into two sub-beams with orthogonal polarizations. An equal intensity and polarization are achieved in the overlapped area of the two sub-beams on the imager by rotating the cube polarizer. The fringe distance can be adjusted by simply moving the Wollaston prism. The interferogram is recorded by an intensified charge coupled device (ICCD) camera (Princeton, PI-MAX), whose gate interval is always 2 ns. The gate is triggered by the DG535 with a suitable delay with respect to the lasers. The spatial resolution of the interferometer is better than 20 μm with a magnification of 7×. A multilayer interference filter is placed in front of the ICCD camera to block the strong broadband emission from the plasma. Shadowgraphs are observed using the same arrangement as the interferometer except that the cube polarizer is rotated to block one of the two sub-beams split by the Wollaston prism.

The energy spectrum of the ions from the Sn plasma is measured with a Faraday cup (FC) from Kimball Physics, which is placed inside the vacuum chamber at a distance of 15 cm from the plasma. The FC is biased with a −30 V dc voltage. The angular distribution of ions could be measured by placing the FC at various angles from 10° to 90° with respect to the target normal.

The in-band CE from laser to 13.5 nm EUV light is measured with an absolutely calibrated EUV energy monitor (E-Mon) from Jenoptik, which consists of a Zr filter, two near-normal-incident multilayer Mo/Si mirrors, and an x-ray photodiode. The CE is integrated over a 2π solid angle. The data from the FC and the E-Mon are acquired, stored, and processed with a digital oscilloscope.

The soft x-ray spectrum from the Sn plasma is observed using a transmission grating spectrometer (TGS), which consists of a 50 μm slit, a 10 000 lines/mm transmission grat-

FIG. 2. Optical schematic illustration of the Nomarski interferometer.

FIG. 4. (Color online) Soft x-ray spectra of EUV plasmas driven by a single (black dot) or a dual pulse (red solid line).
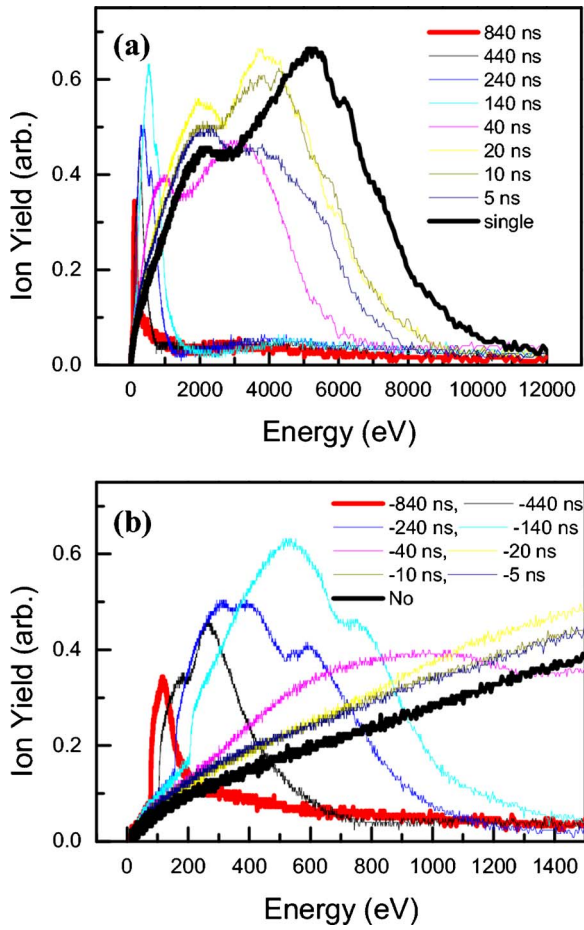

FIG. 3. (Color online) (a) Typical energy spectra of ions from laser-produced Sn plasmas driven by single (black line) and dual-pulses with various delay times (color lines); (b) and expanded spectra from 0 to 1500 eV.

ing, and a back-illuminated x-ray CCD camera (Roper). Its spectral resolution is better than 0.1 nm. Both the E-Mon and the spectrometer are installed in the plane of laser incidence at an angle of 45° with respect to the target normal. The data from the FC, the E-Mon, the TGS, and the interferometer (shadowgraphy) could be simultaneously collected in a single shot.

III. EXPERIMENTAL RESULTS

A. Properties of ion and 13.5 nm EUV light

The ion energy spectrum is deduced from the time of the flight (TOF) measured by the FC. Typical ion energy spectra from the laser-produced Sn plasmas driven by a single pulse (black line) and a dual pulse with various delay times (color lines) are shown in Fig. 3(a). Expanded spectra from 0 to 1500 eV are shown in Fig. 3(b). The intensity of the pumping laser is 2×10^{11} W/cm^2. The energy and pulse duration of the prepulse are 2 mJ and 130 ps, respectively. The FC is placed at 10° with respect to the target normal.

It is seen in Fig. 3(a) that for a single pulse the ion spectrum approximately obeys a Maxwellian distribution, most of the ions are above 2 keV, and the flux peak is located above 5 keV. With the introduction of a prepulse, the shape of the ion spectrum is completely different from that of
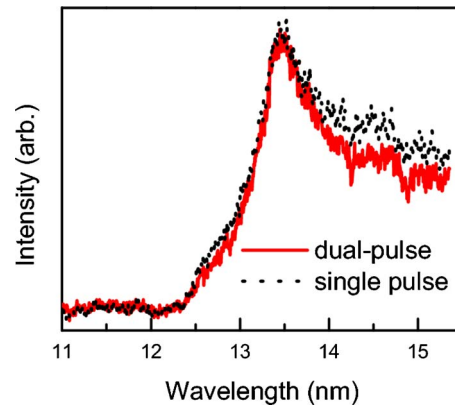
a single pulse. The ions with high energy are significantly mitigated and all ions are shifted towards low energy. The flux peak is shifted towards lower energy with an increase in the delay time. It is seen in Fig. 3(b) that at delay of 840 ns (red line) the flux peak is located at less than 150 eV. Compared with that of a single pulse, more than 30 times reduction in the ion energy of the flux peak is achieved. More than 30 times reduction could be obtained for the whole range from 800 to 1200 ns. Smaller reduction factors are observed with a longer delay time >1200 ns.

The in-band CE was measured simultaneously with the ion spectrum measurements. In the case of a single pulse, CE is 2%. In the case of a dual pulse, CE varies with delay time. It was observed that at delay times from 800 to 1200 ns almost the same CE as that of a single pulse is achieved. So at delay times from 800 to 1200 ns a much lower ion energy and nearly the same in-band CE are simultaneously obtained as compared with those of a single pulse.

The EUV light centered at 13.5 nm with a bandwidth of 2% mainly comes from the unresolved transition array (UTA) of Sn^{8+} to Sn^{13+}, which are in an optimum population in a laser-produced plasma with a temperature around 30 eV.[11–13] The same in-band conversion efficiency reveals almost the same plasma temperature in the EUV emitting region in these two cases. Furthermore, soft x-ray spectra from the Sn plasmas were also observed in the same shots for the measurements of the CE and ion spectrum. Typical spectra of the Sn plasma driven by single (black dot) and dual pulses (red solid line) are shown in Fig. 4. It is seen in Fig. 4 that the two spectra are nearly the same except for the spectral narrowing observed in the case of the dual pulse. This confirms the same in-band CE in the two cases. The spectral narrowing comes from the lower initial density with a dual pulse. This will be discussed later in Sec. IV A.

The effect of the prepulse energy on the reduction in the ion energy was investigated. The ion energy spectra observed with various prepulse energies are shown in Fig. 5. The pulse duration of the prepulse is fixed at 130 ps. It is seen that there is a threshold of prepulse energy to achieve a large reduction factor. It is necessary to have 2 mJ to achieve a 30 times reduction factor under present conditions. Above 2 mJ, the reduction factor is saturated. At the same time, too much energy in the prepulse will result in high energy ions induced
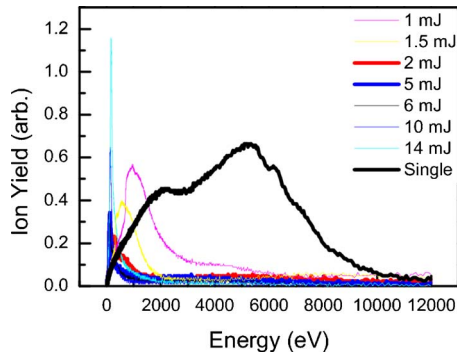
FIG. 5. (Color online) Ion energy spectra from Sn plasmas driven by a dual pulse at various energies of the prepulse.

by the prepulse itself. Note that under present conditions, the focal spot size of the prepulse is much larger than that of the pumping pulse, so the necessary prepulse energy could be reduced further.

The influence of the duration of the prepulse on the reduction in the ion energy was investigated by repeating the experiments with pulse durations from 130 to 600 ps. The required energies of the prepulse to achieve 30 times reduction in the ion energy as a function of the pulse duration are shown in Fig. 6. It is seen that the required energy linearly increases with increasing pulse duration. This confirms that in order to obtain a large reduction factor the intensity of the prepulse must be above some minimum value. This intensity may correspond with the threshold of phase explosion, as discussed in Sec. III B.

The possible mechanism underlying the reduction of ion energy must come from the interaction of the pumping pulse with the preplasma instead of the solid surface. In order to understand the phenomena mentioned above, it is necessary to analyze the interaction of the laser pulse with the preformed plasma. The processes of ion acceleration in laser-produced plasma driven by a dual pulse can be described as follows. Firstly, the prepulse irradiates a solid density target surface. A preplasma is formed and expands into the vacuum. After a delay time, a plasma with a smooth density profile is formed in front of the target surface. Then the pumping pulse is incident onto the preplasma instead of the initial full density surface, and laser energy may be deposited inside the
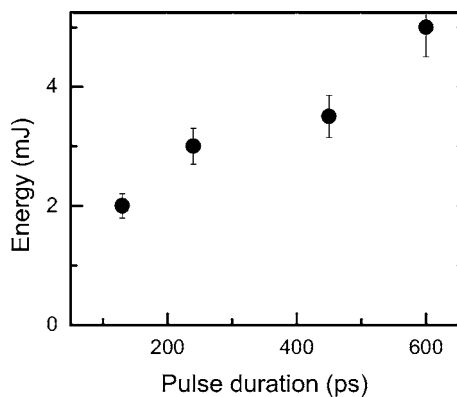

FIG. 6. Necessary prepulse energy to achieve 30 times reduction in the ion energy as a function of pulse duration.
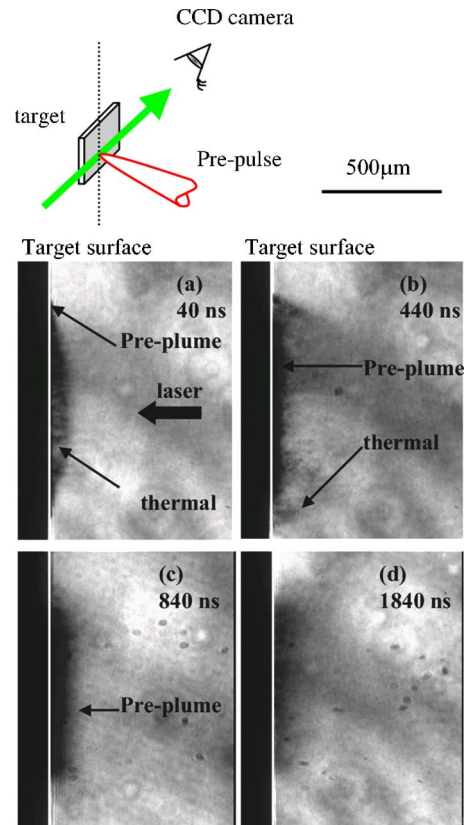

FIG. 7. (Color online) Shadowgraphs of preplasmas obtained at various delay times; (a) 40, (b) 440, (c) 840, and (d) 1840 ns.

preplasma. The preplasma is heated to a suitable temperature to generate 13.5 nm EUV light efficiently, and, finally, the plasma with an initial low density and smooth density profile expands into the vacuum. The ions and neutral particles are accelerated during the plasma expansion.

B. Evolution of the preplasma

The dynamic evolution of a preplasma induced by a prepulse was investigated by time-resolved shadowgraphy and interferometry. Shadowgraphs of the preplasma taken at various delay times of 40, 440, 840, and 1840 ns are shown in Figs. 7(a)–7(d), respectively. The zero point represents the delay time at which the pre- and pumping laser pulses arrive at the target surface at the same time. The energy of the prepulse is 2 mJ. The pumping pulse is blocked. The prepulse comes from the right-hand side of the images shown in Fig. 7.

Obviously, there are two separate parts in the early stages of the preplasma, as shown in Figs. 7(a) and 7(b). One is the well-known thermal plasma with an expansion velocity of 10^6 cm/s; the other part, with a much lower expansion velocity of 10^4 cm/s, is called the preplume hereafter. Accompanying the uniform preplume, a few large size particles are seen in late stages as shown in Figs. 7(c) and 7(d).

The cold preplume may come from the phase explosion of the solid target surface due to the energy transfer from the thermal plasma. Recalling that the focal spot size of the prepulse is 300 μm, the threshold intensity of the prepulse to achieve a large reduction in the ion energy is ~2
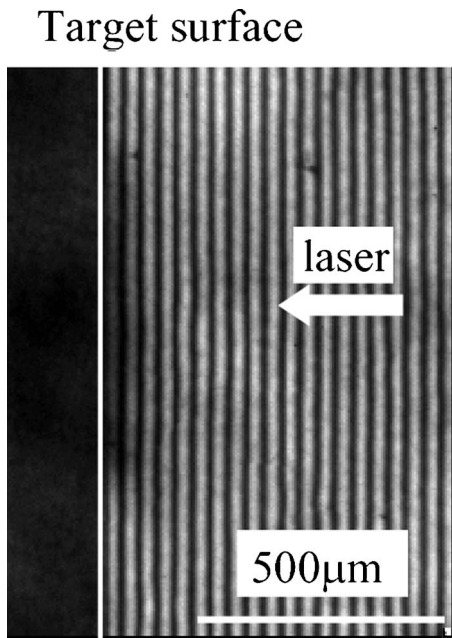
Target surface

FIG. 8. Interferogram of the preplasma observed at delay of 840 ns.

FIG. 9. Density profile of the preplume at delay time of 840 ns.

$\times 10^{10}$ W/cm^2. This intensity is just around the threshold for phase explosion.[14] In this case, the surface is superheated into a liquid phase, and a homogeneous bubble nucleation occurs. As a consequence, the target surface material experiences an abrupt phase transformation from liquid to a mixture of vapor and droplets, which are ejected from the target surface. According to homogeneous nucleation theory, the vapor formation rate can be described as $\exp(-\tau_0/t)$, where τ_0 is the time for the establishment of significant nucleation, which is much longer than the laser pulse duration.[15] So the cold preplume appears several hundred nanoseconds after the prepulse.

However, note that in our experiments, the intensity of the prepulse is controlled just around the threshold intensity for phase explosion, so most of the ablated material is in uniform vapor instead of large size droplets. This can be seen in the shadowgraphs shown in Fig. 7. The uniform vapor expands into the vacuum and a smooth density profile is formed in front of the initial surface after a specific delay time.

It is seen in Figs. 7(c) and 7(d) that after a delay of 840 ns the fast thermal plasma can be neglected. Interferograms of the preplasma at various delay times were obtained with the Nomarski interferometer. A typical interferogram of the preplasma obtained at delay time of 840 ns is shown in Fig. 8. It is seen in Fig. 8 that there is no fringe shift at all. This shows that the preplume is mainly composed of neutral particles at this time.

The density profile of the preplume is deduced from the transmission profile of the probe beam obtained from the shadowgraphs shown in Fig. 7. Assuming that the preplume is uniform laterally, the transmission of the probe beam can be simplified as $I/I_0 = \exp[-4\pi k d\rho(z)/\lambda\rho_0]$, where d the width of the preplume, λ is the wavelength of the probe light in the same units as d, $\rho(z)$ is the density of the preplume at a distance z from the initial target surface, ρ_0 is the density of
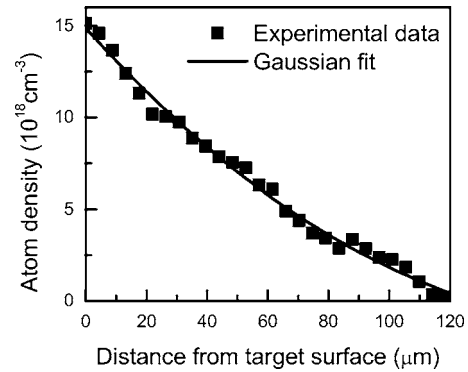
solid Sn, and k is the extinction coefficient. $k=4$ for the 0.532 μm probe light is interpolated from the values shown in Ref. 16. d is 400 μm. A typical density profile of the preplume deduced from the shadowgraph shown in Fig. 7(c) at delay time of 840 ns is shown in Fig. 9 (black square). It is seen in Fig. 9 that the atom density decays from 1.5 $\times 10^{19}$ to 1×10^{18} cm^{-3} when the distance from the initial target surface reaches 120 μm. Laser absorption in a low density plume will be discussed in Sec. IV A. The line in Fig. 9 represents a fit to the experimental data with a Gaussian function.

The length of the preplume increases with increasing delay time. The reduction factor in the energy of the ions at the flux peak as a function of the length of the preplume is shown in Fig. 10. It is seen that the reduction factor increases with the increasing size of the preplume, i.e., the ion energy E_p is inversely proportional to the preplume length l_s, scaling as $E_p \propto 1/l_s$. At longer delay times >1200 ns, the density of the preplume is too low to block the pumping pulse; in this case, most of the laser energy is absorbed by the full density target surface and a small reduction in the ion energy is observed.

C. Dynamics of the EUV plasma

To clarify the mechanism dominating ion acceleration and EUV light generation in the interaction of the pumping laser pulse with the preplume, the density profile of the EUV plasma was measured using the Nomarski interferometer. Typical interferograms of laser-produced Sn plasmas driven
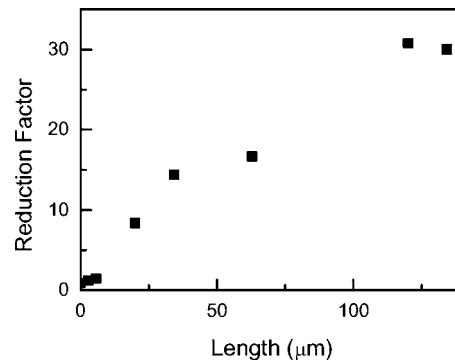

FIG. 10. Reduction factor in the ion energy as a function of the scale length of the preplume.
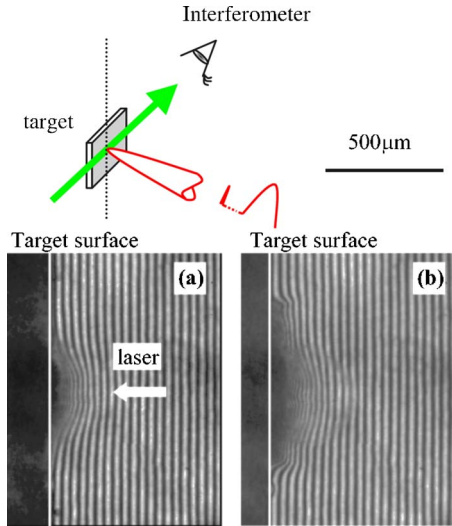
FIG. 11. (Color online) Interferograms of the EUV plasmas driven by (a) single and (b) dual pulses.

by a single and a dual pulse are shown in Figs. 11(a) and 11(b), respectively. The pumping laser intensity is 2×10^{11} W/cm^2, and the energy of the prepulse is 2 mJ with a delay time of 840 ns. The interferograms are taken at 2 ns after the peak of the pumping laser. The laser is incident from the right-hand side of the imagesas shown in Fig. 11.

A comparison between Figs. 11(a) and 11(b) shows that in the case of dual pulse the fringe shift induced by the EUV plasma is farther away from the target surface as compared with that of a single pulse, which reveals that the EUV plasma driven by a dual pulse may take place within the preplume. A phase shift map was deduced from the interferograms using a mathematical treatment based on fast Fourier transform (FFT), and a plasma density profile was deduced from the phase shift map with the Abel inversion by assuming that the EUV plasma obeys cylindrical symmetry.[17] Figure 12 shows typical density profiles of laser-produced Sn plasmas driven by a single laser pulse (red dot) and a dual pulse (black square) deduced from the interferograms shown in Figs. 11(a) and 11(b), respectively. Both of them can be fitted by an exponential decay function $\exp(-x/l_s)$ with scale lengths of 100 and 110 μm, where $l_s = c_s t$, and $c_s = \mathrm{SQRT}(ZT_e/M_i)$ is the sound velocity, and T_e, Z, and M_i are
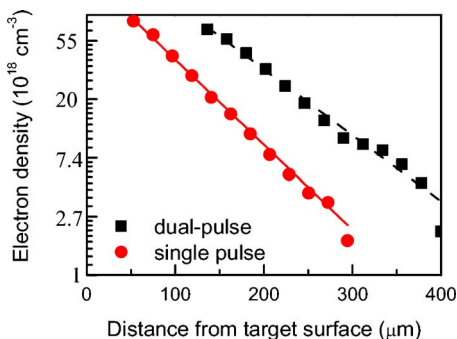

FIG. 12. (Color online) Density profiles of the EUV plasmas driven by single (red dot) and dual pulses (black square); the red solid line represents the exponential fit to data of a single pulse and the black dashed line is the exponential fit to the data of a dual pulse.

the plasma temperature, the average charge state, and the ion mass, respectively. It is seen that the whole density profile of the EUV plasma driven by a dual pulse is shifted farther away from the initial target surface as compared with that driven by a single pulse. This shift confirms the assumption that most of the main laser pulse is deposited inside the preplume instead of the infinitely sharp, full density surface in the case of a dual pulse.

Except for different absolute distances from the target surface, the two density profiles look similar. However, recalling that in the case of the dual pulse the pumping laser is deposited in a preformed plume with a Gaussian density profile with a length of 120 μm, the plasma irradiated by a single pulse should expand faster than that irradiated by a dual pulse. A higher ion energy should be observed in the case of a single pulse. This coincides with the ion measurements mentioned above.

A higher plasma temperature deduced from the faster expansion in the case of a single pulse conflicts with the measurements of the CE and the soft x-ray spectrum mentioned in Sec. III A. The possible reason may come from the fact that both the CE and the spectrum are spatially and temporally integrated. In the case of the single pulse, the laser is absorbed in a higher density, more laser energy is absorbed, and a higher plasma temperature is formed in the higher density region in the rising slope of the laser pulse, so faster expansion results. But due to the opacity effect of the Sn plasma to 13.5 nm EUV light,[18–20] most of the 13.5 nm EUV light can only escape from the low density Sn plasma after a significant plasma expansion.[21] So the detected properties of the 13.5 nm EUV light are almost the same for single and dual pulses.

IV. DISCUSSION

A. Absorption of the laser pulse in the low density preplume

Under our experimental conditions, the dominant absorption mechanism is inverse bremsstrahlung (IB). An estimate of laser absorption in the corona using the IB absorption coefficient can be obtained from[22]

$$f_A = 1 - \exp\left(-\frac{8}{3}\frac{\nu_{ei}l_s}{c}\cos^3\theta\right) \tag{1}$$

where $\nu_{ei} \approx 3 \times 10^6 \ln \Lambda Z n_e / T_e^{3/2}$ is the electron-ion collision frequency, l_s is the scale length of the plasma, c is the velocity of light in vacuum, θ is the incidence angle, n_e is the plasma density, and $\ln \Lambda$ is the Coulomb logarithm.

Equation (1) predicts that a laser can be efficiently absorbed in a cold and high electron density plasma region. In general, it is commonly accepted that most of the absorption locally occurs near the critical density. However, for a long laser pulse (such as nanoseconds several), a plasma with a large scale length (hundred micrometers) formed in the laser incidence line is still cool enough that IB is very strong, so that the absorption takes place over a wide density range from well underdense to the critical density instead of localized at the critical density surface.[23]

Due to the opacity of the Sn plasma to 13.5 nm EUV emission, efficient 13.5 nm EUV light comes from the well underdense region in laser-produced Sn plasmas.[17] Even though less EUV emission is generated in the underdense plasma region due to the lower ion density, more EUV light can escape due to the lower opacity, in which case the detectable output of the EUV light is almost same as the full density case. So almost the same CE is observed in both single and dual-pulse cases.

The spectral narrowing in the dual-pulse case mentioned in Sec. III A also comes from the initially lower and smoother plasma density. The out-of-band emission comes from the transitions of Sn ions with lower and higher charger states beyond 8+ and 13+. The spectral width is related to the charge state distribution of the Sn ions. An initially lower and smoother density could reduce the charge state transfer induced by collisions among the ions during the plasma expansion. Then a narrower spectrum is observed in the case of the dual pulse. This also coincides with observations of low-density Sn-doped foam, SnO_2, and targets with low Sn concentration.[24–27]

In the case of the dual pulse, laser energy is deposited in the preformed plume with a smooth density profile. The ablation pressure is reduced with a smooth initial density profile, because the laser is absorbed in the lower densities farther from the ablation surface. The ablation pressure could induce the ejection of neutral particles from the substrate of the target. So the reduction in the ablation pressure is helpful to reduce the generation of neutral particles.

B. Ion acceleration in the expansion of plasma with an initially smooth density profile

In order to understand the significant reduction in the energy of ions from the Sn plasma driven by a dual pulse, the expansion of the plasma is discussed. It is known that ion acceleration comes from charge separation formed during the plasma expansion. In the case of a single pulse, the initial plasma is an infinitely sharp boundary; the maximum electric field associated with the electron Debye sheath can be described as $E=k_BT_e/e\lambda_{DE}$, where T_e is the electron temperature, $\lambda_{D0}=(\varepsilon_0 k_B T_{e0}/Zn_{i0}e^2)^{1/2}$ is the initial local Debye length, and n_{i0} is the initial ion density.[6] However, for the dual-pulse case at suitable delay times (800–1200 ns), the preplume has a density length l_s much larger than λ_{DE}, i.e., $l_s \gg \lambda_{DE}$. Then the associated maximum electric field becomes $E=k_BT_e/el_s$. Hence the ion acceleration depends on the initial density profile. Ions with lower energy should result from an initially smooth density profile.

Mora[5] and Grismayer and Mora[6] have theoretically investigated the influence of the initial ion density profile on the plasma expansion. They showed that for a Gaussian plasma with a size much larger than the Debye length, fast electron cooling during the adiabatic expansion results in a strong reduction in ion acceleration as compared with that of a sharp boundary. Since the characteristic time for electron cooling approximately scales with the size of the preplasma, a significant reduction of electron temperature should be observed in the case of a smooth initial density profile.

Even with a plasma scale length of $80\lambda_{De0}$, the numerical model only predicts a twofold difference in velocity, i.e., four times in energy between an infinitely sharp target surface and a finite density gradient.[5] However, a reduction factor of 30 in the ion energy was observed in our experiments. Furthermore, the theoretical model predicted that there is no large difference during the isothermal expansion between the cases of the smooth density profile and the sharp boundary.[5] But as mentioned in Sec. III C, in the case of the single pulse the EUV plasma expands faster than that of the dual pulse during the laser pulse.

Therefore, further experimental efforts are necessary to characterize the whole process of plasma expansion—both isothermal and adiabatic expansion phases. Comparing the detailed experimental data with the theoretical work carried out at the specified experimental conditions could significantly improve our understanding of the basic plasma physics dominating ion acceleration.

V. SUMMARY

In summary, efforts to clarify the interaction of a laser pulse with a preformed Sn plume for an EUV ultraviolet lithography light source were carried out. The significant reduction in the ion energy and the nearly equal in-band CE from laser to 13.5 nm EUV light observed in the case of the dual pulse could be explained by the interaction of the pumping pulse with a preplume having a smooth density profile induced by the prepulse. The preplume has a Gaussian density profile. The ion energy scales with the length of the preplume, as $E_p \propto 1/l_s$. The lower and smoother initial density profile reduces the density gradient of the EUV plasma, such that slower expansion and slower ions result in the case of a dual pulse. At the same time, because of the opacity effect of the Sn plasma, the 13.5 nm EUV light mainly escapes from well underdense plasma, so the CE's are almost same in the two cases. This provides a convenient way to control the ion kinetic energy in laser plasma interaction. Further experimental and theoretical efforts are necessary to characterize the whole processes of plasma expansion in detail and to understand the physics contributing to ion acceleration in plasma with an initially smooth density profile.

ACKNOWLEDGMENTS

[1] P. J. Silverman, J. Microlithogr., Microfabr., Microsyst. **4**, 011006 (2005).
[2] Y. Shimada, *et al.* Appl. Phys. Lett. **86**, 051501 (2005).
[3] J. P. Allain *et al.*, Proc. SPIE **5751**, 1110 (2005).
[4] P. Mora, Phys. Rev. Lett. **90**, 185002 (2003).
[5] P. Mora, Phys. Plasmas **12**, 112102 (2005).
[6] T. Grismayer and P. Mora, Phys. Plasmas **13**, 032103 (2006).
[7] A. J. Mackinnon *et al.*, Phys. Rev. Lett. **86**, 1769 (2001).
[8] K. Matsukado *et al.*, Phys. Rev. Lett. **91**, 215001 (2003).
[9] Y. Tao and M. S. Tillack, Appl. Phys. Lett. **89**, 111502 (2006).
[10] Y. Tao, S. S. Harilal, M. S. Tillack, K. L. Sequoia, B. O'Shay, and F. Najmabadi, Opt. Lett. **31**, 2492 (2006).
[11] A. Cummings *et al.*, J. Phys. D **37**, 2376 (2004).
[12] G. O'Sullivan *et al.*, Proc. SPIE **5196**, 273 (2004).
[13] C.-S. Koay, S. George, K. Takenoshita, R. Bernath, E. Fujiwara, M. Ri-

chardson, and V. Bakshi, Proc. SPIE **5751**, 279 (2005).

[14] J. Ren, X. Yin, S. S. Orlov, and L. Hesselink, Appl. Phys. Lett. **88**, 061111 (2006); J. H. Yoo, S. H. Jeong, X. L. Mao, R. Greif, and R. E. Russo, *ibid.* **76**, 783 (2000); J. H. Yoo, S. H. Jeong, X. L. Mao, R. Greif, and R. E. Russo, J. Appl. Phys. **88**, 1638 (2000); Q. Lu, S. S. Mao, and R. E. Russo, Appl. Phys. Lett. **80**, 3072 (2002).

[15] M. S. Tillack, D. Blair, and S. S. Harilal, Nanotechnology **15**, 390 (2004).

[16] E. D. Palik, *Handbook of Optical Constants of Solids III* (Academic, San Diego, 1998).

[17] Y. Tao *et al.*, Appl. Phys. Lett. **86**, 201501 (2005).

[18] Y. Tao *et al.*, Appl. Phys. Lett. **85**, 1919 (2004).

[19] T. Aota and T. Tomie, Phys. Rev. Lett. **94**, 015004 (2005).

[20] S. Fujioka *et al.*, Phys. Rev. Lett. **95**, 235004 (2005).

[21] Y. Tao *et al.*, Appl. Phys. Lett. **87**, 241502 (2005).

[22] W. L. Kruer, *The Physics of Laser Plasma Interactions* (Addison-Wesley, New York, 1988).

[23] J. S. De Groot, S. M. Cameron, K. Mizunoa, K. G. Estabrook, R. P. Drake, W. L. Kruer, and P. E. Young, Phys. Fluids B **3**, 1241 (1991); J. S. De Groot, K. G. Estabrook, W. L. Kruer, R. P. Drake, K. Mizuno, and S. M. Cameron, *ibid.* **4**, 701 (1992).

[24] T. Okuno *et al.*, Appl. Phys. Lett. **88**, 161501 (2006).

[25] S. S. Harilal, M. S. Tillack, Y. Tao, B. O'Shay, R. Paguio, and A. Nikroo, Opt. Lett. **31**, 1549 (2006).

[26] H. W. Choi *et al.*, J. Opt. Soc. Am. B **17**, 1616 (2000).

[27] G. D. O'Sullivan and R. Faulkner, Opt. Eng. (Bellingham) **33**, 3978 (1994).